The influence of level ice on the frequency domain response of floaters

Keijdener, Chris; de Oliveira Barbosa, João Manuel; Metrikine, Andrei V.

DOI
10.1016/j.coldregions.2017.09.004

Publication date
2017

Document Version
Accepted author manuscript

Published in
Cold Regions Science and Technology

Citation (APA)
Keijdener, C., de Oliveira Barbosa, J. M., & Metrikine, A. V. (2017). The influence of level ice on the frequency domain response of floaters. *Cold Regions Science and Technology*, *143*, 112-125. https://doi.org/10.1016/j.coldregions.2017.09.004

The influence of level ice on the frequency domain response of floaters

Chris Keijdener[a,b,*], João Manuel de Oliveira Barbosa[a], Andrei Metrikine[a,b]

[a] *Delft University of Technology, Stevinweg 1, 2628CN, Delft*
[b] *SAMCoT, Department of Civil and Transport Engineering, NTNU, NO-7491 Trondheim*

Abstract

In this paper the effect of a nearby, semi-infinite, level ice sheet on the frequency domain response of a thin, floating, rigid body is studied using a 2D model. The ice is modeled using a dynamic Euler-Bernoulli beam and the finite depth water layer is described with the Laplace equation and the linearized Bernoulli equation. Eigenfunction matching is used to resolve the interface between the ice covered and open water regions.

The body is excited by external loads, generating waves. The waves are partially reflected by the ice edge and these reflected waves influence the body's response. It is this influence that this paper focuses on. Below a certain onset frequency the amplitude of the reflected waves is insignificant and consequently the body remains unaffected by the ice. This frequency is only sensitive to the ice thickness with thinner ice resulting in a higher onset frequency.

Above the onset frequency the reflected waves cause quasi-standing waves between body and ice. For frequencies at which half the wavelength of the surface wave in the water is approximately an integer multiple of the gap length, the amplitude of the standing waves is greatly amplified. This can result in (anti-)resonance depending on the phasing between the reflected waves and the body's motion.

Keywords: Ice-floater interaction, hydrodynamics, level ice, frequency domain response

1. Introduction

Although the interest in offshore Arctic hydrocarbons has declined in recent times, it is still a great prospect for our future. The water depths encountered in large parts of the Arctic offshore region make floating structures the main platform for drilling and production. Understanding the interaction between ice and floaters is therefore paramount in performing the eventual extraction of those resources in a safe and sustainable way.

Ice-floater interaction (IFI) is a challenging problem because of the many disciplines it combines and is further complicated by the complex material properties of sea ice (Timco and Weeks, 2010). Although full scale data is mostly limited to ice breakers and the drilling vessel Kulluk (Wright, 2001), theoretical studies have been going on for several decades (Palmer and Croasdale, 2013).

IFI has three main components: the ice, the floater and the fluid. Focus is often on the ice with the floater assumed to be immovable and rigid. The interaction is then governed by the ice and takes place through the contact. However, for the design of station-keeping systems the dynamics of the floater is of importance. Allowing the floater to move adds a second path of interaction in addition to the contact, namely through the fluid. Quite often this coupling is not included because it involves solving a coupled hydrodynamics (HD) problem.

[1] This paper addresses the hydrodynamic coupling between vessel and ice. The focus is placed on the effect of the presence of level ice on the frequency domain response of the floating vessel. The fundamental question we answer is whether the open-water response of the floater is applicable in the presence of ice. The coupling investigated in this paper has been addressed in very few studies and, therefore, its effect remains largely unexplored.

[1] Two fields of research are closely associated with the type of coupling addressed in this paper, namely the field of ice-structure interaction and the field of wave propagation in and wave reflection from ice. In the former the focus has mostly been placed on the mechanical aspects of the interaction, namely on the vessel excitation by the contact with ice and the resulting failure of the ice. Hydrodynamics has been incorporated in the sense that its effect on these mechanical aspects has been studied. To the author's knowledge the most advanced model to date that includes hydrodynamics is by Valanto (2001), who solved the 3D interaction between a forward advancing ice breaker and an ice plate. The comparison with full-scale data was very satisfactory. In this model however, the vessel was kinematically prescribed to move forward at a constant speed.

[1] Few studies have included hydrodynamic coupling between vessel and ice. Tsarau et al. (2014) studied the coupling between a floater and nearby ice rubble and found good agreement with model tests performed in a wave tank. They did not include the effect of the surface waves

*Corresponding author. Tel.: +31 15 278 6899
Email address: c.keijdener@tudelft.nl (Chris Keijdener)

though. In Su et al. (2010) a numerical model was introduced for the interaction between an ice breaker with three degrees of freedom and level ice but hydrodynamic coupling was not accounted for either. A more rigorous approach is to use CFD but this results in extreme computation times and hardware requirements. This was done by Gagnon (2007) and Gagnon and Wang (2012) to study the collision between an iceberg and a loaded tanker.

[1] Overall it can be concluded that in this field the amount of studies on the hydrodynamic coupling between vessel and ice is limited and no qualitative studies on the coupling have been done.

[1] In the closely related field of waves in ice infested waters the interaction between ocean waves and ice sheets is studied. This field has had a steady activity since the 1990's, Squire (1995), and has seen a resurgence in the last two decades (Squire, 2007). By its very nature this field has incorporated hydrodynamics from the very beginning but its goal has been to understand the wave processes that go on in marginal ice zone (MIZ). The focus was placed on understand the reflection and transmission of ocean waves by the ice. This process, in combination with the resulting break-up of the ice, is essential in understanding the attenuation of waves as they propagate through the MIZ. Some of the findings in this field are that when waves are at normal incidence to an ice edge, at low frequencies nearly all energy is transmitted into the ice sheet and is almost fully reflected back into the sea at high frequencies Fox and Squire (1990). For oblique waves a critical angle exists beyond which no waves propagate into the ice (Fox and Squire, 1994). In both these studies the reflection by the draft of the ice was ignored, an assumption of minor consequences as shown in, for instance, (Williams and Squire, 2008). Lastly (Chung and Linton, 2005) studied the effect of a gap between two adjacent semi-infinite ice sheets. In this case the reflection coefficient becomes periodic, having a series of resonance peaks at regular intervals. When a vessel operates in the presence of ice, the waves it radiates will also be reflected by the ice, which associates the problem considered in this paper to the work by Chung and Linton.

[1] Because of the apparent lack of studies in this overlapping region between the research fields, this work aims to improve our understanding of the hydrodynamic coupling (HD) coupling between a floater and flexible level ice. To this end a very common IFI scenario is studied, namely the dynamics of a floater in the vicinity of level ice. The main questions to be answered are:

- How is the frequency domain response of the floater that is excited by a sinusoidal load affected by the presence of a flexible level ice sheet located in close proximity of the floater?
- Under which circumstances can the floater-ice coupling be neglected?

As this paper aims at obtaining qualitative answers to the above-formulated questions, the problem is restricted to a two dimensional vertical plane and the floater is assumed to be thin. Although the response in the presence of level ice will be quantitatively different for each floater, it is postulated that the phenomenon observed and understanding gained from this simple model are applicable to a broader range of floaters.

In the next section the adopted mathematical model is defined. After this the solution strategy is explained in sections 3 and 4. The results are then discussed in section 5 and lastly conclusions and recommendations are given in section 6.

2. Model description

The problem to be solved is depicted in Figure 1. A rigid body, whose thickness is small compared to the water depth, floats on the surface of the fluid layer. At a distance l from the body there is a floating ice sheet that extends to negative infinity. The goal is to determine the body's vertical and rotational motion caused by time harmonic forces or moments acting on it, while accounting for the presence of the ice sheet.

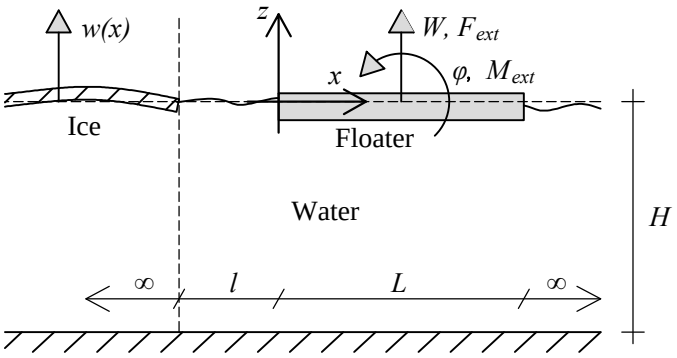

Figure 1: The waves generated by the body's motion reflect at the ice-open water interface. The pressure exerted by the reflected waves alter the body's response.

The model is assumed 2D, which means that the out-of-plane dimension of the body is much bigger than the distance to the floating ice sheet. This scenario may be representative of the heave and roll motions of barges, tabular icebergs or large pieces of ice rubble. The extension to three-dimensional bodies would allow for more accurate analysis of other motion types, like pitch and yaw and would lift the restriction on the out-of-plane dimension of the body. The extension to embedded bodies (i.e., without ignoring the draft) would enable the analysis of horizontal motions, such as surge and sway and allow a more complex geometry of the body to be considered.

The body is excited by external loads. These push it against the fluid, which in turn offers resistance to the body's motion. Waves are generated at the body-fluid interface, and propagate away from it, see figure 2 on the

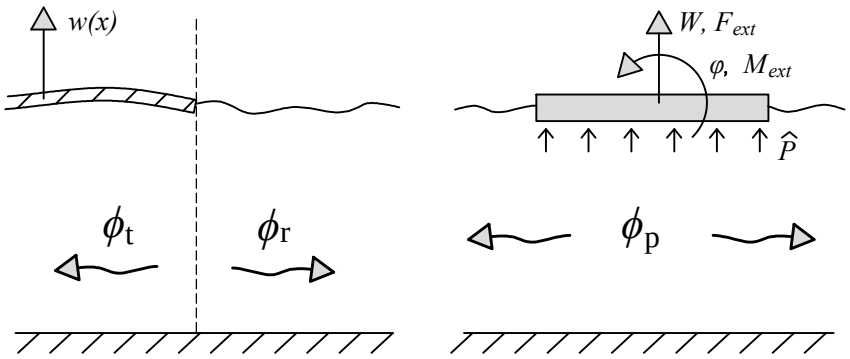

Figure 2: Excitation of the body generates waves (right image) which are party reflected and transmitted by the ice sheet (left image)

right. Waves that propagate to the right, find no heterogeneity and therefor do not return to the body. On the contrary, waves propagating to the left will encounter the ice sheet and will be partially transmitted and partially reflected at the ice edge, see figure 2 on the left. The response of the floating body is affected by the reflected wave field. The influence of the reflected waves on the body's response is the main subject of this paper. In the ensuing the mathematical problem is formulated and in the next section the solution method is discussed.

Since the results are studied in the frequency domain, all equations presented in this paper have already been transformed to that domain, denoted by a tilde accent. The Fourier transform used can be found in Appendix A, Eq. (A.1).

2.1. Body's governing equations

The forces acting on the body are the external force $F_{\text{ext}} = \tilde{F}_{\text{ext}} e^{i\omega t}$ and moment $M_{\text{ext}} = \tilde{M}_{\text{ext}} e^{i\omega t}$ and the interaction pressure $\hat{p}(x)$ acting along the interface with the fluid. The equation of motion (EOM) of the body is therefore:

$$-\omega^2 \begin{bmatrix} m & 0 \\ 0 & J \end{bmatrix} \begin{bmatrix} \tilde{W} \\ \tilde{\varphi} \end{bmatrix} \tag{1}$$

$$= -\int_0^L \begin{bmatrix} \hat{p}(x) \\ (x - C_{\text{x}})\hat{p}(x) \end{bmatrix} dx + \begin{bmatrix} \tilde{F}_{\text{ext}} \\ \tilde{M}_{\text{ext}} \end{bmatrix} \tag{2}$$

where m is the body's mass, J its rotational inertia, $\tilde{W}$ its heave motion, $\tilde{\varphi}$ its rotational motion, L its length and C_{x} the x-coordinate of its center of gravity. The integral on the right-hand side converts the distributed fluid pressure into equivalent forces and moments with respect to the center of gravity of the body.

The unknowns of this system of equations are the displacement $\tilde{W}$, rotation $\tilde{\varphi}$ and the interaction pressure $\hat{p}$. On its own the system is undetermined and must be coupled to the fluid to relate the vessel's displacements with the resulting interaction pressure. The fluid governing equations are described next.

2.2. Fluid's governing equations

The fluid is assumed to be incompressible, inviscid and irrotational allowing it to be described by the Laplace equation:

$$\nabla^2 \tilde{\phi} = 0 \qquad \forall\ x \in (-\infty, \infty)\ \cap\ z \in (-H, 0) \tag{3}$$

where parentheses denote an open interval and brackets, in formulas to follow, a closed one. The *displacement* potential $\tilde{\phi}(x, z)$ is defined by:

$$\vec{u} = \nabla \phi \tag{4}$$

where $\vec{u}$ contains the horizontal and vertical displacements of the fluid. [2] A displacement potential (see for instance Jensen et al. (2011)) is used as it results in a clearer and more standard notation from a structural dynamics point of view.

The governing equation of the fluid must be accompanied by proper boundary conditions (BC) in order for the system to be determined. At the lower boundary, $z = -H$, the BC prevents penetration of the fluid into the seabed. This translates into the vertical displacements of the fluid to be zero:

$$\left.\frac{\partial \tilde{\phi}}{\partial z}\right|_{z=-H} = 0 \qquad \forall\ x \in (-\infty, \infty) \tag{5}$$

At the upper boundary, $z = 0$, the fluid pressure $\tilde{p}$ must balance with the external pressure. The fluid pressure is calculated according to the linearized Bernoulli equation [3] for unsteady potential flow (Stoker, 1992):

$$\tilde{p}(x, z) = -\rho_w b \left(-\omega^2 \tilde{\phi} + g \left(\frac{\partial \tilde{\phi}}{\partial z} + z \right) \right) \tag{6}$$

where ρ_w is the fluid density and g is the gravitational constant. [3] The first term in Eq. (6) introduces linear hydrodynamic effects, whereas the second term is responsible for the hydrostatic effects. The dynamic pressure term was removed by the linearization.

The external surface pressure acting on the fluid surface is position dependent. Under the ice sheet the fluid

pressure must be equal to that imposed by the dynamically flexible ice (which is modeled as an Euler-Bernoulli Beam). Under the rigid body the pressure is equal to the interaction pressure $\hat{p}(x)$ defined in the previous sub-section and outside these regions the pressure is zero (as the atmospheric pressure is ignored). In this way, the boundary pressure at $z = 0$ is:

$$\tilde{p}(x,0) = \begin{cases} -\omega^2 \rho_i A \tilde{w}(x) + EI\tilde{w}''''(x) & \forall\ x \in (-\infty, -l] \\ 0 & \forall\ x \in (-l, 0] \\ \hat{p}(x) & \forall\ x \in (0, L] \\ 0 & \forall\ x \in (L, \infty) \end{cases} \tag{7}$$

where [4] $w(x)$ is the vertical displacements of the ice, ρ_i is the density of the ice, A its cross-sectional area, $\tilde{w}(x)$ its transverse displacements, E its Young's modules, I its second moment of area and the prime denotes a spatial derivative. Solving the beam equation requires four BCs. Two of them are related to the radiation at infinity, which enforce that no energy propagates from infinity and that the beam's deflection is bounded at infinity. The other two are related to the stress free edge of the ice (free of moments and shear forces):

$$EI\tilde{w}''|_{x=-l} = 0 \tag{8a}$$

$$EI\tilde{w}'''|_{x=-l} = 0 \tag{8b}$$

To ensure a continuity of vertical displacements of ice and fluid the following kinematic interface condition (IC) applies:

$$\tilde{w}(x) = \left.\frac{\partial\tilde{\phi}(x,z)}{\partial z}\right|_{z=0} \qquad \forall\ x \in (-\infty, -l] \tag{9}$$

A similar kinematic IC applies between body and fluid. However, since the body is rigid the vertical displacements caused by its rotations have to be included:

$$\tilde{W} + (x - C_\mathrm{x})\tilde{\varphi} = \left.\frac{\partial\tilde{\phi}}{\partial z}\right|_{z=0} \qquad \forall\ x \in (0, L] \tag{10}$$

For convenience, the fluid is divided into two regions: the ice-covered region, $x \leq -l$, and the open-water region, $x > -l$, see Figure 1. In the open-water region two potentials are used: $\tilde{\phi}_p$ to capture the waves radiated by the body and ϕ_r to capture the waves that are reflected by the ice. In the ice-covered region a single potential $\tilde{\phi}_t$ is used to capture those radiated waves that are transmitted into the ice-covered region; all waves in this region either propagate towards negative infinity or, in case of evanescent modes, decay exponentially with the distance from the ice edge.

Based on this definition the interaction pressure $\hat{p}(x)$ is accounted for by $\tilde{\phi}_p$. Consequently, $\tilde{\phi}_r$ will satisfy the pressure release condition at the surface for all $x > -l$. However, while satisfying the kinematic IC between body and fluid, Eq. (9), the summation of both potentials has to be used because both contribute to the vertical displacements at the surface.

$\tilde{\phi}$ thus is composed of three potentials and their spatial dependence is:

$$\tilde{\phi}(x,z) = \begin{cases} \tilde{\phi}_t(x,z) & \forall\ x \in (\infty, -l] \\ \tilde{\phi}_p(x,z) + \tilde{\phi}_r(x,z) & \forall\ x \in (-l, \infty) \end{cases} \quad \cap\ z \in [-H, 0] \tag{11}$$

To ensure compatibility and continuity between the two regions, two extra ICs need be satisfied along their interface:

$$\tilde{\phi}_\mathrm{t}\Big|_{x=-l} = \left(\tilde{\phi}_\mathrm{p} + \tilde{\phi}_\mathrm{r}\right)\Big|_{x=-l} \qquad \forall\ z \in [-H, 0] \tag{12a}$$

$$\left.\frac{\partial\tilde{\phi}_\mathrm{t}}{\partial x}\right|_{x=-l} = \left(\frac{\partial\tilde{\phi}_\mathrm{r}}{\partial x} + \frac{\partial\tilde{\phi}_\mathrm{p}}{\partial x}\right)\Bigg|_{x=-l} \qquad \forall\ z \in [-H, 0] \tag{12b}$$

The first one ensures a continuity of fluid pressure while the second one a continuity of horizontal displacements.

The methodology used for solving the defined problem is discussed next.

3. Discretization

An analytical solution to the problem as defined above is difficult because of the integral in the body's EOM (Eq. (1)) and the spatial dependence of the IC between body and fluid (Eq. (10)). To overcome this difficulty both equations are discretized, starting with the interaction pressure. The discretization strategy used in this paper is similar to the boundary element method.

3.1. Discretization of the interaction pressure

The integral in Eq. (1) cannot be evaluated directly because the interaction pressure $\hat{p}(x)$ is unknown. The pressure is distributed continuously between $(0, L]$ and so can be seen as working on infinitely many points. This condition is relaxed by approximating the continuous pressure with a summation of elements. To illustrate the discretization procedure, figure 3 shows a fictitious continuous pressure profile, depicted by the dashed line. This continues profile is approximated by the summation of Θ elements, analogous to a Riemann sum. [5] The approximation in figure 3 uses eight such elements, i.e. $\Theta = 8$. These elements are indexed with α. For convenience, the pressure is assumed invariant within each element. Increasing the number of elements lets the approximation converge to the exact solution.

Figure 4 shows the pressure exerted by a single element on the fluid. The pressure, with amplitude P_α, is applied within the domain of the element $(x_\alpha - \Delta_\mathrm{x}, x_\alpha + \Delta_\mathrm{x}]$. The element is centered around $x_\alpha = (\alpha - 1/2)2\Delta_\mathrm{x}$ and has a width Δ_x. This surface pressure excites the fluid, thereby

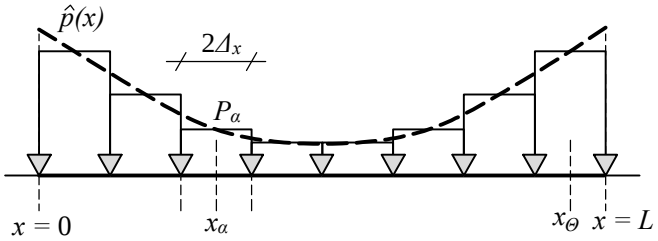

Figure 3: The interfacial pressure is discretized using 8 elements, analogous to the Riemann sum. Within each element α the pressure is constant and proportional to $\tilde{P}_\alpha$.

generating waves which are captured by the potential $\tilde{\phi}_\alpha$. Since each element generates its own set of waves, the total response of the fluid is given by the combined effect of all elements and so:

$$\tilde{\phi} = \sum_{\alpha=1}^{\Theta} \tilde{\phi}_\alpha \tag{13}$$

After discretization, the integrals over the hull of the body in Eq. (1) can be evaluated:

$$\int_0^L \hat{p}(x)\ \mathrm{d}x = 2\Delta_\mathrm{x} \sum_{\alpha=1}^{\Theta} \tilde{P}_\alpha \tag{14a}$$

$$\int_0^L (x - C_\mathrm{x})\hat{p}(x)\ \mathrm{d}x = 2\Delta_\mathrm{x} \sum_{\alpha=1}^{\Theta} r_\alpha \tilde{P}_\alpha \tag{14b}$$

where $r_\alpha = x_\alpha - C_\mathrm{x}$.

Approximating the continuous profile with the Riemann sum has reduced the number of unknowns to the Θ unknown complex amplitudes $\tilde{P}_\alpha$. The goal is now to obtain these amplitudes, allowing the interaction problem to be solved. Doing this requires the fluid response generated by each element: $\tilde{\phi}_\alpha$. These potentials are derived after the discretization of the IC.

3.2. Discretization of the kinematic body-fluid interface condition

The second equation that has to be discretized is the IC in Eq. (10). Just like the interaction pressure the IC also applies continuously between $(0, L]$. Discretizing the IC will result in a finite number of conditions that need to be satisfied.

The discretization of the pressure introduced Θ unknowns so enforcing the IC the same amount of times results in the same number of equations as there are unknowns, making the problem solvable. This is done by enforcing an equivalent IC within the domain of each element. There are multiple ways to do this. In this paper the average vertical displacement (AVD) within each element is matched to the AVD of the body within the element's domain. Using this strategy the IC in Eq. (10) is replaced by the following set of Θ equations, indexed with β:

$$\begin{aligned}\frac{1}{2\Delta_\mathrm{x}} \int_{x_\beta-\Delta_\mathrm{x}}^{x_\beta+\Delta_\mathrm{x}} \left(\tilde{W} + (x - C_\mathrm{x})\tilde{\varphi}\right)\ \mathrm{d}x \\ = \frac{1}{2\Delta_\mathrm{x}} \int_{x_\beta-\Delta_\mathrm{x}}^{x_\beta+\Delta_\mathrm{x}} \left.\frac{\partial\tilde{\phi}(x,z)}{\partial z}\right|_{z=0} \mathrm{d}x \\ = \tilde{w}_\beta \qquad \forall\ \beta = 1\,..\,\Theta\end{aligned} \tag{15}$$

where the symbol $\tilde{w}_\beta$ is given to the fluid's AVD within element β. Due to the discretization of the pressure, the fluid response $\tilde{\phi}$ is given by the superimposed response of all elements (see Eq. (13)) and so the IC becomes:

$$\begin{aligned}\tilde{W} + r_\beta\tilde{\varphi} = \frac{1}{2\Delta_\mathrm{x}} \sum_{\alpha=1}^{\Theta} \int_{x_\beta-\Delta_\mathrm{x}}^{x_\beta+\Delta_\mathrm{x}} \left.\frac{\partial\tilde{\phi}_\alpha(x,z)}{\partial z}\right|_{z=0} \mathrm{d}x \\ = \sum_{\alpha=1}^{\Theta} \tilde{w}_{\alpha,\beta} \qquad \forall\ \beta = 1\,..\,\Theta\end{aligned} \tag{16}$$

where the integral on the left hand side resulted in the arm $r_\beta = x_\beta - C_\mathrm{x}$ and the symbol $\tilde{w}_{\alpha,\beta}$ designates the contribution of element α to the AVD within element β.

In the next section the discretized problem is solved and the body's response is obtained.

4. Solving the problem

The discretization performed in the previous section resulted in Θ discrete potentials $\tilde{\phi}_\alpha$, each capturing the fluid response generated by the surface pressure of the corresponding element α as depicted in figure 4. The next step in solving the problem is to find an expression for each $\tilde{\phi}_\alpha$.

4.1. Fluid response due to each element's surface pressure

The reflection and transmission processes described before also occur when the waves generated by each element hit the ice and so each $\tilde{\phi}_\alpha$ also consists of three potentials:

$$\tilde{\phi}_\alpha = \begin{cases} \tilde{\phi}_{\mathrm{t},\alpha} & \forall\ x \in (\infty, -l]\ \cap\ z \in [-H, 0] \\ \tilde{\phi}_{\mathrm{p},\alpha} + \tilde{\phi}_{\mathrm{r},\alpha} & \forall\ x \in (-l, \infty)\ \cap\ z \in [-H, 0] \end{cases} \tag{17}$$

where $\tilde{\phi}_{\mathrm{p},\alpha}$ is the potential associated with the waves radiated by element α of the body whereas $\tilde{\phi}_{\mathrm{r},\alpha}$ satisfies the pressure release condition in the whole region $x \in (-l, \infty)$. The three potentials are depicted in figure 4. Finding $\tilde{\phi}_\alpha$ therefore implies finding its three constituents.

The final form of each of the three potentials is presented next. As the focus of the paper is on the results rather than the methodology the derivations have been moved to the appendices.

The final expression of $\tilde{\phi}_{\mathrm{p},\alpha}$ is shown below. The full derivation based on the Residue Theorem can be found in

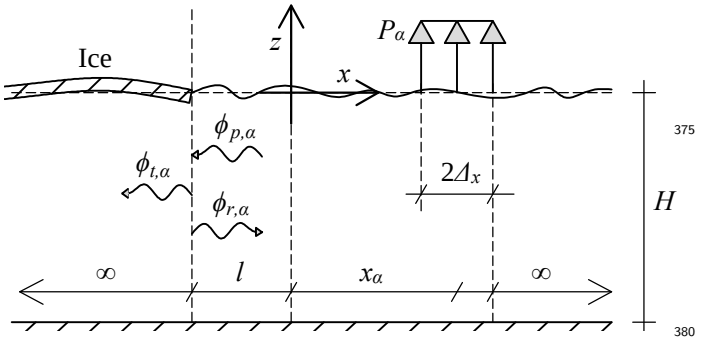

Figure 4: The generation of a transmitted and reflected potential due to the presence of the ice.

Appendix A.

$$\tilde{\phi}_{\mathrm{p},\alpha}(x,z) = -\frac{\tilde{P}_\alpha}{\rho_w g}\sum_{n=0}^{N}\gamma_n Q_n^{-1} I_{n,\alpha}(x) Z_n(z) \quad \forall\ x \in (-l,\infty)\ \cap\ z \in [-H,0] \tag{18}$$

where γ_n is related to [6] the type of contour used for each root. All roots use a circular shaped contour that fully encloses its singularity. However, the root $k=0$ lays on the real axis and thus on the integration path and so has to be omitted using Cauchy principle value. This results in a half-circle rather than a full circle. Consequently its magnitude is halved resulting in the following definition for γ_n:

$$\gamma_n = \begin{cases} 1/2, & \text{if } n = 0 \\ 1, & \text{if } n > 0 \end{cases} \tag{19}$$

Q_n is the derivative of $\omega^2/g - k\tanh(kH)$ for $k = k_n$:

$$Q(k) = \left(\omega^2/g - k\tanh(kH)\right) - k\left(kH\,\mathrm{sech}^2(kH) + \tanh(kH)\right) \tag{20}$$

$I_{n,\alpha}(x)$ captures the rectangular shape of the pressure elements is given by:

$$I_{n,\alpha}(x) = \mathrm{sgn}(x_1(x))\mathrm{e}^{\mathrm{i}k_n|x_1(x)|} - \mathrm{sgn}(x_2(x))\mathrm{e}^{\mathrm{i}k_n|x_2(x)|} \tag{21}$$

where $x_1(x) = x - (x_\alpha + \Delta_\mathrm{x})$ and $x_2(x) = x - (x_\alpha - \Delta_\mathrm{x})$ [6] capture the distance with respect to the boundaries of each element and the depth Eigenfunction $Z_n(z)$ ensures the solution satisfies the Laplace equation and the BC at the seabed. It is given by:

$$Z(z) = \cosh(k(z+H))\cosh^{-1}(kH) \tag{22}$$

where $Z_n(z) = Z(z)|_{k=k_n}$ and lastly the summation is taken over the k_n wavenumbers that satisfy the following dispersion relation:

$$\omega^2/g - k\tanh(kH) = 0 \tag{23}$$

k_n is defined as:

- k_0: 0 (generated by the rectangular shape of the pressure element)
- k_1: the negative real pole (propagating mode) of Eq. (23) where the Sommerfeld radiation condition was used to eliminate the positive real pole
- $k_n, n \geq 2$: the imaginary poles (evanescent modes) of Eq. (23) located in the upper half-plane (UHP) in ascending order

In this expression for $\tilde{\phi}_{\mathrm{p},\alpha}(x,z)$ there is only one unknown; $\tilde{P}_\alpha$.

It is important to note that the solution sums over N modes. In actual fact there are infinitely many modes which satisfy the equations governing $\tilde{\phi}_{\mathrm{p},\alpha}$ but this infinite set was truncated at N for practical reasons. The numerical value of N is determined based on the convergence of the results.

Next, general expressions for the potentials $\tilde{\phi}_{\mathrm{t},\alpha}$ and $\tilde{\phi}_{\mathrm{r},\alpha}$ are presented. These satisfy the governing equation (Eq. (3)) and the BC at the seabed (Eq. (5)). The potentials satisfy different surface conditions; $\tilde{\phi}_{\mathrm{t},\alpha}$ balances the fluid pressure with the pressure in the ice and $\tilde{\phi}_{\mathrm{r},\alpha}$ satisfies the pressure release condition. Eigenfunction matching is then used to get these general expression to satisfy the ICs at $x = -l$, given by Eqs. (8) and (12). This will result in an expression for their modal amplitudes.

First, the general solution for $\tilde{\phi}_{\mathrm{r},\alpha}$ is presented. Within the domain of definition of this potential, $x > -l$, the surface boundary condition in Eq. (7) simplifies to the pressure release condition, i.e. $\tilde{p} = 0$ (the external forcing from the pressure element has already been accounted for by $\tilde{\phi}_{\mathrm{p},\alpha}$). The solution, derived in Appendix B, is:

$$\tilde{\phi}_{\mathrm{r},\alpha}(x,z) = \sum_{n=1}^{N} a_{n,\alpha}\mathrm{e}^{\mathrm{i}k_n(x+l)}Z_n(z) \quad \forall\ x \in [-l,\infty)\ \cap\ z \in [-H,0] \tag{24}$$

where all amplitudes $a_{n,\alpha}$ are unknown and i is the imaginary unit. It is important to note that $\tilde{\phi}_{\mathrm{r},\alpha}$ sums over the same modes as $\tilde{\phi}_{\mathrm{p},\alpha}$, albeit with different amplitudes, as both potentials satisfy the same surface boundary conditions and consequently the same dispersion relation.

Lastly, the general solution for the transmitted potential is presented. For this potential the surface condition reduces to a balance between fluid pressure and the pressure imposed by the Euler-Bernoulli beam used to model the ice. As shown in Appendix C, this potential can be represented as:

$$\tilde{\phi}_{\mathrm{t},\alpha}(x,z) = \sum_{m=1}^{M} \bar{a}_{m,\alpha}\mathrm{e}^{-\mathrm{i}\bar{k}_m(x+l)}\bar{Z}_m(z) \quad \forall\ x \in (-\infty,-l]\ \cap\ z \in [-H,0] \tag{25}$$

where all $\bar{a}_{m,\alpha}$ are unknown, $M = N + 2$ and $\bar{Z}_m(z) = Z(z)|_{k=\bar{k}_m}$. [7] Because of the presence of the ice this potential satisfies a different surface condition then $\tilde{\phi}_{\mathrm{p},\alpha}$ and $\tilde{\phi}_{\mathrm{r},\alpha}$, its roots have to satisfy a different dispersion relation. The fluid modes in the ice-covered region are thus different from those in the open-water region. The bar accent is used to highlight terms affected by this different set of modes. The set of roots $\bar{k}_m$ that can exist in the ice-covered region is defined as:

- $\bar{k}_{1,2}$: the complex poles located in the upper half-plane which are related to the bending modes of the beam
- $\bar{k}_3$: the negative real pole (propagating fluid mode) related to surface waves of the water layer where the Sommerfeld radiation condition was used to eliminate the positive real pole
- $\bar{k}_m, m \geq 4$: the countably infinite imaginary poles (evanescent fluid modes) from the upper half-plane in ascending order

With solutions for all three potentials the IC at $x = -l$ can be resolved. This is done using Eigenfunction matching, performed in Appendix D, similar too (Montiel et al., 2012). During this process expressions are found for the unknown amplitudes $a_{n,\alpha}$ and $\bar{a}_{m,\alpha}$ and these amplitudes become proportional to the excitation of $\tilde{\phi}_{\mathrm{p},\alpha}$ at $x = -l$. [8] At this point all potential have become proportional to the unknown $\tilde{P}_\alpha$'s.

The response of the fluid due to each pressure element, including the effects of the ice, has now been obtained in the form of $\tilde{\phi}_\alpha$. The only remaining unknowns are now the Θ $\tilde{P}_\alpha$'s and the body's response. The only remaining equations still to be satisfied are the interface between body and fluid, Eq. (10), and the body's EOM, Eq. (1). All remaining unknowns are found in the next subsection.

4.2. Resolving the body-fluid interface

Now that an expression has been found for $\tilde{\phi}_\alpha$, the body-fluid IC can be applied. This will result in an expression for each $\tilde{P}_\alpha$. The last step is then to solve the EOM of the body, thereby obtaining the response of the body and concluding the derivation.

The body-fluid IC was discretized in Eq. (15). It states that the fluid's vertical displacement averaged over element β's domain, i.e. $\tilde{w}_\beta$, should be equal to the body's AVD within the same domain. As the fluid response is given by the combined effect of all elements, see Eq. (13), the contribution of each element α to the AVD of each interfacial element β is needed, see Eq. (16). These contributions are represented by the symbol $\tilde{w}_{\alpha,\beta}$. After obtaining all contributions they can be summed to obtain the AVD of the fluid $\tilde{w}_\beta$:

$$\tilde{w}_\beta = \sum_{\alpha=1}^{\Theta} \tilde{w}_{\alpha,\beta} \qquad \forall\ \beta = 1\,..\,\Theta \tag{26}$$

To find an expression for $\tilde{w}_{\alpha,\beta}$ the integral in Eq. (16) has to be evaluated. Because the body is always located to the right of the ice, $\tilde{\phi}_\alpha$ reduces to the summation of $\tilde{\phi}_{\mathrm{p},\alpha}$ and $\tilde{\phi}_{\mathrm{r},\alpha}$ within the domain of the body (see Eq. (17)). Substituting this into Eq. (16) gives:

$$\begin{aligned}\tilde{w}_{\alpha,\beta} &= \tilde{w}_{\mathrm{p},\alpha,\beta} + \tilde{w}_{\mathrm{r},\alpha,\beta} \\ &= \frac{1}{2\Delta_\mathrm{x}} \int_{x_\beta-\Delta_\mathrm{x}}^{x_\beta+\Delta_\mathrm{x}} \left(\frac{\partial\tilde{\phi}_{\mathrm{p},\alpha}}{\partial z} + \frac{\partial\tilde{\phi}_{\mathrm{r},\alpha}}{\partial z} \right)\Bigg|_{z=0} \mathrm{d}x\end{aligned} \tag{27}$$

The contribution of $\tilde{\phi}_{\mathrm{r},\alpha}$ to element β's AVD is:

$$\begin{aligned}&\tilde{w}_{\mathrm{r},\alpha,\beta} = \\ &\frac{1}{2\Delta_\mathrm{x}} \sum_{n=1}^{N} \frac{a_{n,\alpha}}{\mathrm{i}k_n} \left(\mathrm{e}^{\mathrm{i}k_n(l+x_\beta+\Delta_\mathrm{x})} - \mathrm{e}^{\mathrm{i}k_n(l+x_\beta-\Delta_\mathrm{x})} \right) \lambda_n\end{aligned} \tag{28}$$

where $\lambda_n = Z_n'(0) = k_n \tanh(k_n H)$. The contribution of $\tilde{\phi}_{\mathrm{p},\alpha}$ is:

$$\tilde{w}_{\mathrm{p},\alpha,\beta} = \frac{2\tilde{P}_\alpha}{\rho_w g} \sum_{n=0}^{\infty} \gamma_n Q_n^{-1} \lambda_n \Gamma_{n,\alpha,\beta} \tag{29}$$

where $\mathrm{sinc}(x) = \sin(x)/x$ and $\Gamma_{n,\alpha,\beta}$ is given by:

$$\Gamma_{n,\alpha,\beta} = \begin{cases} \mathrm{e}^{\mathrm{i}\Delta_\mathrm{x}k_n}\,\mathrm{sinc}(\Delta_\mathrm{x}k_n), & \text{if } \alpha = \beta \\ i\Delta_\mathrm{x}k_n \mathrm{e}^{2i\Delta_\mathrm{x}k_n|\alpha-\beta|}\,\mathrm{sinc}^2(\Delta_\mathrm{x}k_n), & \text{if } \alpha \neq \beta \end{cases} \tag{30}$$

As each $\tilde{w}_{\alpha,\beta}$ scales linearly with its $\tilde{P}_\alpha$ (see Eq. (18), (D.9) and (D.10)), $\tilde{P}_\alpha$ can be factored out to get:

$$\begin{aligned}\tilde{w}_\beta &= \sum_{\alpha=1}^{\Theta} \tilde{w}_{\mathrm{p},\alpha,\beta} + \tilde{w}_{\mathrm{r},\alpha,\beta} = \\ &\sum_{\alpha=1}^{\Theta} (\tilde{\Lambda}_{\mathrm{p},\alpha,\beta} + \tilde{\Lambda}_{\mathrm{r},\alpha,\beta})\tilde{P}_\alpha \qquad \forall\ \beta = 1\,..\,\Theta\end{aligned} \tag{31}$$

All Θ equations are now combined into matrix form:

$$\tilde{\mathbf{w}} = (\tilde{\mathbf{\Lambda}}_\mathrm{p} + \tilde{\mathbf{\Lambda}}_\mathrm{r})\tilde{\mathbf{P}} = \tilde{\mathbf{\Lambda}}\tilde{\mathbf{P}} \tag{32}$$

where $\tilde{\mathbf{w}}$ and $\tilde{\mathbf{P}}$ are $\Theta \times 1$ vectors containing the AVD and pressure of all elements and $\tilde{\mathbf{\Lambda}}_\mathrm{p}$, $\tilde{\mathbf{\Lambda}}_\mathrm{r}$ and $\tilde{\mathbf{\Lambda}}$ are $\Theta \times \Theta$ matrices relating the two. [9] Since $\tilde{\phi}_{\mathrm{p},\alpha}$ is shift-invariant in x, $\tilde{\mathbf{\Lambda}}_\mathrm{p}$ is a symmetric Toeplitz matrix and thus only requires Θ evaluations to fill. Due to the dependence on l, $\tilde{\phi}_{\mathrm{r},\alpha}$ is not shift-invariant making $\tilde{\mathbf{\Lambda}}_\mathrm{r}$ a "normal" symmetric matrix requiring $(\Theta-1)^2/2 + \Theta$ evaluations to fill.

The IC given in Eq. (16) can be rewritten into matrix form:

$$\mathbf{1}\tilde{W} + \mathbf{r}\tilde{\varphi} = \tilde{\mathbf{w}} \tag{33}$$

where $\mathbf{1}$ and $\mathbf{r}$ are $\Theta \times 1$ vectors, the former filled with 1's and the latter containing all Θ arms r_β. Combining this equation with Eq. (32) and solving for $\tilde{\mathbf{P}}$ result in:

$$\tilde{\mathbf{P}} = \tilde{\mathbf{\Lambda}}^{-1}(\mathbf{1}\tilde{W} + \mathbf{r}\tilde{\varphi}) = \tilde{\boldsymbol{\kappa}}\tilde{W} + \tilde{\boldsymbol{\kappa}}_\varphi\tilde{\varphi} \tag{34}$$

where the $\Theta \times 1$ vectors $\tilde{\boldsymbol{\kappa}}$ and $\tilde{\boldsymbol{\kappa}}_\varphi$ represent the frequency dependent effective heave and pitch stiffnesses of the fluid layer.

Having obtained a relation between the fluid pressure and body's response the last step in obtaining the coupled response is to solve Eq. (34) together with the EOM of the body. This is done in the next subsection.

4.3. Body's response

Now that a relation between the amplitudes $\tilde{P}_\alpha$ and the bodies motion's has been found its EOM can be solved. The integrals in the EOM (Eq. (3)) were evaluated in Eqs. (14) which can be rewritten in matrix form:

$$2\Delta_{\mathrm{x}} \sum_{\alpha=1}^{\Theta} \tilde{P}_\alpha = 2\Delta_{\mathrm{x}} (\tilde{\mathbf{P}} \cdot \mathbf{1}) \tag{35a}$$

$$2\Delta_{\mathrm{x}} \sum_{\alpha=1}^{\Theta} \tilde{P}_\alpha r_\alpha = 2\Delta_{\mathrm{x}} (\tilde{\mathbf{P}} \cdot \mathbf{r}) \tag{35b}$$

Substituting these solutions into the EOM of the body (Eq. (1)) yields:

$$-\omega^2 \begin{bmatrix} m & 0 \\ 0 & J \end{bmatrix} \begin{bmatrix} \tilde{W} \\ \tilde{\varphi} \end{bmatrix} = 2\Delta_{\mathrm{x}} \begin{bmatrix} \tilde{\mathbf{P}} \cdot \mathbf{1} \\ \tilde{\mathbf{P}} \cdot \mathbf{r} \end{bmatrix} + \begin{bmatrix} \tilde{F}_{ext} \\ \tilde{M}_{\mathrm{ext}} \end{bmatrix} \tag{36}$$

Rewriting the interaction forces in terms of the effective stiffnesses introduced in Eq. (34) gives:

$$-\omega^2 \begin{bmatrix} m & 0 \\ 0 & J \end{bmatrix} \begin{bmatrix} \tilde{W} \\ \tilde{\varphi} \end{bmatrix} \tag{37}$$

$$= 2\Delta_{\mathrm{x}} \begin{bmatrix} \tilde{\boldsymbol{\kappa}} \cdot \mathbf{1} & \tilde{\boldsymbol{\kappa}}_\varphi \cdot \mathbf{1} \\ \tilde{\boldsymbol{\kappa}} \cdot \mathbf{r} & \tilde{\boldsymbol{\kappa}}_\varphi \cdot \mathbf{r} \end{bmatrix} \begin{bmatrix} \tilde{W} \\ \tilde{\varphi} \end{bmatrix} + \begin{bmatrix} \tilde{F}_{\mathrm{ext}} \\ \tilde{M}_{\mathrm{ext}} \end{bmatrix} \tag{38}$$

$$= 2\Delta_{\mathrm{x}} \tilde{\mathbf{K}} \begin{bmatrix} \tilde{W} \\ \tilde{\varphi} \end{bmatrix} + \begin{bmatrix} \tilde{F}_{\mathrm{ext}} \\ \tilde{M}_{\mathrm{ext}} \end{bmatrix} \tag{39}$$

Solving this set of equations gives the unknown amplitudes gives:

$$\begin{bmatrix} \tilde{W} \\ \tilde{\varphi} \end{bmatrix} = \left(-\omega^2 \begin{bmatrix} m & 0 \\ 0 & J \end{bmatrix} - 2\Delta_{\mathrm{x}} \tilde{\mathbf{K}} \right)^{-1} \begin{bmatrix} \tilde{F}_{\mathrm{ext}} \\ \tilde{M}_{\mathrm{ext}} \end{bmatrix} \tag{40}$$

The frequency response function of the heave and rotational motion have now been obtained. This frequency response function includes both the effect of the immediate fluid response through $\tilde{\boldsymbol{\Lambda}}_{\mathrm{p}}$ and the effect of the waves reflected by the ice through $\tilde{\boldsymbol{\Lambda}}_{\mathrm{r}}$, see Eq. (32). By replacing $\tilde{\boldsymbol{\Lambda}}$ by $\tilde{\boldsymbol{\Lambda}}_{\mathrm{p}}$ in Eq (34) and then solving the body's EOM the ice effect can be removed and the response of the body in open water can be obtained. This allows for easy comparison between the cases when ice is present and when it is not. In the next section the ice's effect on the floater's response is studied by comparing these two cases.

5. Results

The goal of this paper is to study the changes in the frequency domain response of the body due to the presence of the ice. In this section these changes are studied by comparing the body's response in the presence of ice with its response in open water. The difference between the two scenarios will be referred to as the *ice effect*.

The frequency response matrix (given by Eq. (40)) is complex valued and frequency dependent. It captures both the amplitude of the body's vibration and the phase lag of the body's response with respect to the harmonic loading. In this paper only the amplitude of the response is focused upon and so the absolute value of the response is studied.

As the ice is only present on one side of the body, the problem is not symmetric in space. [10] The reflected waves only come from the left side and so exert an assymetric pressure on the body that integrates to a non-zero moment. This implies that even if the vessel is only excited in heave, after some time the reflected waves will also cause a rotational motion. The ice thus couples heave and rotational motion of the body.

[10] The body is acted upon by two two excitations: an external vertical force $\tilde{F}_{\mathrm{ext}}$ and moment $\tilde{M}_{\mathrm{ext}}$. These excite the heave motion $\tilde{W}$ and rotation $\tilde{\varphi}$. Consequently there are three items to discuss; 1) the heave response due to the external force, given the symbol $\tilde{W}_F$, 2) the rotation due to the external moment, $\tilde{\varphi}_M$ and 3) the coupling terms $\tilde{W}_M = \tilde{\varphi}_F$.

For convenience the magnitude of the loads is chosen such that the resulting quasi-static responses of $\tilde{W}_F$ and $\tilde{\varphi}_M$ are of unit amplitude:

$$\tilde{F}_{\mathrm{ext}} = \rho_w g L \qquad \rightarrow \ |\tilde{W}_F|_{\omega=0} = 1 \text{ [m]} \tag{41a}$$

$$\tilde{M}_{\mathrm{ext}} = \frac{\rho_w g L^3}{12} \qquad \rightarrow \ |\tilde{\varphi}_M|_{\omega=0} = 1 \text{ [rad]} \tag{41b}$$

For computing the results the following set of parameters are used unless specified otherwise: $g = 9.81$ m/s^2, ice thickness $h = 1$ m, $A = h$ (rectangular cross-section), $I = 1/12h^3$, $\rho_i = 925$ kg/m^3, $E = 5$ GPa, $H = 100$ m, $\rho_w = 1025$ kg/m^3, $l = 15$ m, $C_{\mathrm{x}} = L/2$, $m = 1\mathrm{E}5$ kg and $L = 30$ m. The thickness of the body is assumed to be negligible and so $J = m/12L^2$. [2] The default values of the environmental parameters (h, ρ_i, E and H) were set to mean values observed in nature. For the remaining parameters it is more difficult to set default value. For this reason parametric studies will be done to investigate their influence over a range that was deemed realistic.

Lastly, based on the convergence of the results, $N = 1000$ modes and the number of elements Θ is set to $\Theta = \lceil \Delta_L L \rceil$ where Δ_L is set to 4 elements per meter. [11] From internal testing it was established that this is sufficiently dense to guarantee a converged response of the body for the cases addressed in this paper. [2] Because an element density is used rather than a fixed number, the error is

independent of L and so the numerical error remains of constant order of magnitude when performing sensitivity study on L.

First the response due to the force is studied and then due to the moment.

5.1. Excitation by the force

The [12] magnitude of the heave $\tilde{W}_F$ and rotational $\tilde{\varphi}_F$ motion induced by the harmonic force $\tilde{F}_{\text{ext}}$ are shown in figure 5. The superscript i denotes response of the body

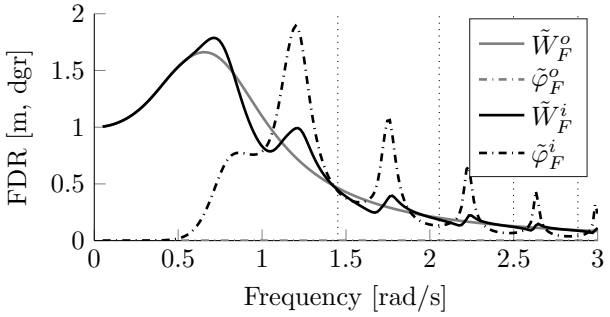

Figure 5: The vertical lines are related to the recurrence rate of the peaks and is discussed later.

in the presence of ice and the superscript o gives that in open water. The difference between the two is the ice effect. The body itself is symmetric and so $\tilde{\varphi}_F^o$ is zero for all frequencies.

Two things stand out when looking at this figure: 1) below a certain frequency the ice has a negligible effect and 2) above this frequency the ice has a significant effect and results in a series of peaks. These observations are explained sequentially.

5.1.1. No ice effect at low frequencies

The reason for the body to remain unaffected at low frequencies lies in the reflection and transmission of the waves incident to an ice edge. Research into this field started in the 1960's. An overview of the earlier work is given by Fox and Squire (1990). A resurgence of activity has taken place in the last two decades (Squire, 2007). In these works it is concluded that, when waves are at normal incidence to an ice edge, at low frequencies nearly all energy is transmitted into the sheet and almost fully reflected back into the sea at high frequencies.

A corresponding type of behavior can also be seen in figure 5. Below a frequency of roughly 0.5 [rad/s] almost no waves are reflected and, consequently, the body is not effected by the ice. The frequency at which the ice effect becomes perceptible is defined as the onset frequency (OF). The OF is defined as the frequency at which the reflection coefficient $\mathfrak{R}$ of an incoming propagating surface wave k_1 first exceeds 1%. The evanescent modes decay very rapidly in space and so their effect on the response of the body is assumed to be negligible. Because of this only the propagating surface wave is considered. This is indeed the same definition of the reflection coefficient given in (Fox and Squire, 1990).

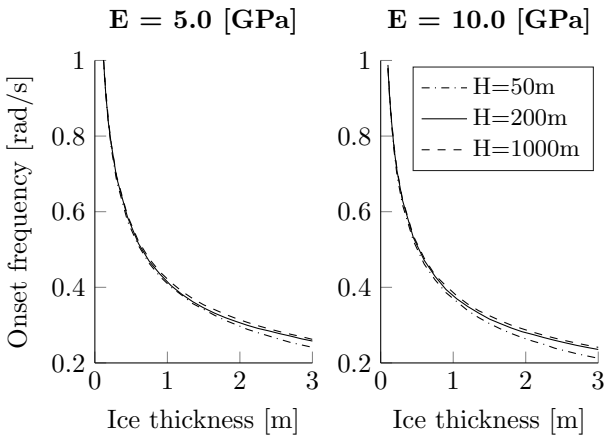

Figure 6: The OF for a range of ice parameters.

In figure 6 the OF is shown as a function of ice thickness. The sensitivity of the OF to various parameters was checked. Of all the environmental parameters in this model only the ice thickness, its Young's modulus and the water depth have a large natural variance. Figure 6 shows that of these three only the ice thickness has a significant influence on the OF. This behavior is consistent with that found in (Fox and Squire, 1990). The following power functions give an accurate fit of the dependence of the OF on the ice thickness for the two cases where $H = 200$ m:

$$\omega_{\text{of}} = \begin{cases} 0.46898h^{-0.3811} - 0.0531 & \text{if } E = 5 \text{ GPa} \\ 0.4183h^{-0.3882} - 0.0391 & \text{if } E = 10 \text{ GPa} \end{cases} \quad (42)$$

with an RMS of 0.0026 and 0.0017 [rad/s] respectively.

Two conclusions can be drawn related to the OF. Firstly, up to the OF the body is unaffected by the ice as seen in [13] figure 5. This implies that if a body has a low natural frequency most of its response occurs at frequencies below the OF and consequently the ice effect will be minimal. This is further enhanced by thin ice as this greatly increases the OF. Secondly, above the OF the ice effect is proportional to the amplitude of the body's vibration in open water, see figure 5. If the amplitude above the OF is small then the ice effect will be small as well. Figure 6 can thus be used to estimate whether a particular body is susceptible to ice effects based on its open water response.

It is important to note that the 2D nature of the model in combination with the simplistic geometry of the body mean that the above formulated results should only be viewed as a first step towards understanding hydrodynamic coupling between ice and body. Also when the gap between ice and body becomes very small evanescent modes might affect the response of the body which will affect the OF.

To sum up, the OF in combination with a body's open water response can be used to estimate the susceptibility

of that body to the ice effect. Only the ice thickness has a significant effect on the OF.

5.1.2. The ice effect after the onset frequency

In the frequency band above the onset frequency the ice effect starts to have a pronounced effect on the response of the body. The most interesting effect is the appearance of the resonance peaks, see figure [13] figure 5, at a series of frequencies. The periodicity of these peaks is characterized by the following equation:

$$2l = \frac{2\pi}{|k_1(\omega)|} j \qquad \forall\ j = 1 \ldots \infty \tag{43}$$

[14] where the absolute value negates the negative sign of k_1. Each frequency found this way is related to the frequency dependent wavelength of the wavenumber k_1 being an integer multiple of twice the gap length. k_1 is the only propagating surface wave contained in the set k_n and is therefor the only root of interest at larger distances from the body. These frequencies are shown in figures 5 and 7 with the dotted lines.

Figure 5 shows that there are well-defined frequency bands wherein the response is altered by the reflected waves. When the body oscillates it loses energy in the form of radiated waves and some of this energy is trapped in the gap between the body and ice in the form of standing wave and the response of the whole system in general. Within these frequency bands the wavelength of the propagating surface wave approximately coincides with the gap length and the amount of energy trapped is greatly increased, dramatically amplifying the amplitude of the standing waves.

These quasi-standing waves, of which the nodes oscillate slightly about the positions that can be divised based on Eq. (43), are visualized in figure 7. The frequencies at which their amplitudes increases coincide with the frequencies at which the resonance amplification of the response is seen in figure 5. Standing waves are characterized by the quasi-sinusoidal patterns seen in figure 7 at some frequencies. Propagating waves are characterized by a constant color in the same figure.

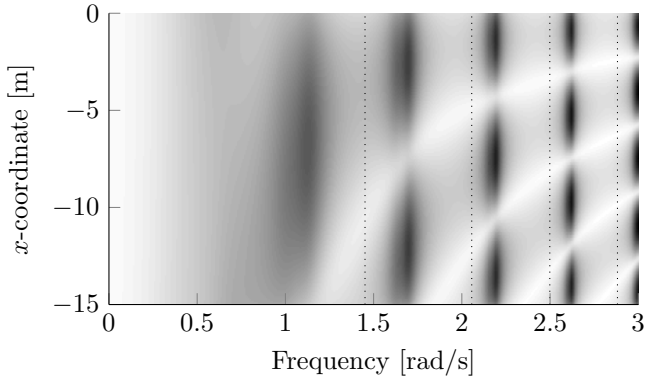

Figure 7: The surface amplitude within the gap for different frequencies. White represents a small amplitude, black a large.

In addition to the standing waves the phasing of the reflected waves is also important. When the reflected waves are in-phase with the vertical motions of the body, resonance occurs and the body's response increases. If the reflected waves are in anti-phase with the body, anti-resonance occurs and its response lowers.

The combined effect of standing waves and (anti-)resonance results in the alterations seen in figure 5. When standing waves occur the rotational motions are greatly amplified because the standing waves occur only on one side of the body and are thus asymmetric in space, exerting a moment and causing the vessel to rock. For the heave motions (anti-)resonance can be seen when the standing waves occur.

5.1.3. Influence of the body's mass

The influence of the body's mass on the ice effect is checked next. This is shown in figure 8. Although the range of masses shown in the figure goes into the unphysical regime, as they would cause the body to sink, it is interesting to check what effect these high masses have. To reduce the ice effect to a single value the root mean squared (RMS) over the frequency range of $[0, 3]$ rad/s is used.

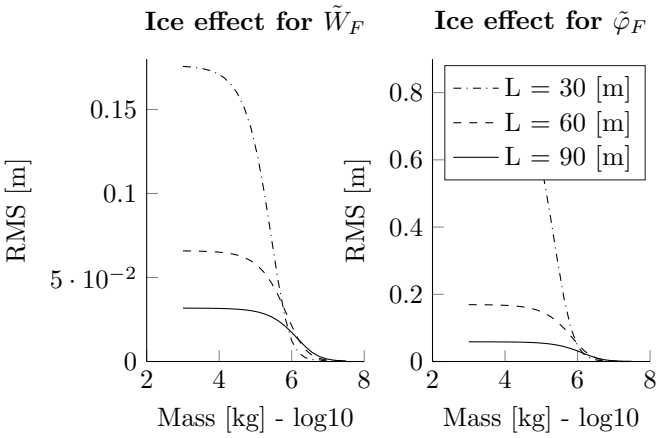

Figure 8: The effect of the body's mass on the ice effect.

Figure 8 clearly shows that increasing the mass lowers the ice effect. As the mass of the body increases while the fluid pressure exerted by the reflected waves remain the same, their overall influence on the response of the body lowers. Increasing the mass reduces the magnitude of the peaks but the frequencies at which they occur remain unaltered. This is supported by Eq. (43).

5.1.4. Influence of the gap length

The last parameter whose effect will be investigated herein is the gap length l. The range that will be checked is $[0, L]$. The larger the ratio l/L, the more important 3D effects become making the results of this 2D model less accurate. For this reason an upper bound of L is used. Special attention is given to the case when ice and body

are almost in contact, i.e. $l \to 0$. Figure 9 shows the influence of l on the ice effect.

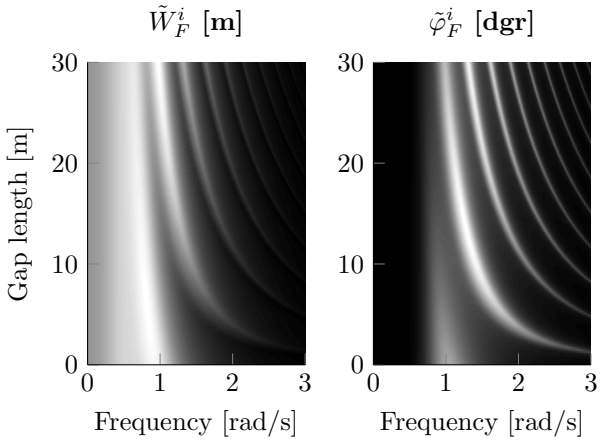

Figure 9: The effect of the gap length l on the response with nearby ice. White is a large amplitude and black a small.

Two things stand out in the figure. Firstly increasing l reduces the spacing between the peaks and introduces more of them. This is consistent with Eq. (43). Secondly, the body's response is affected by the ice when $l = 0$ as shown in figure 10.

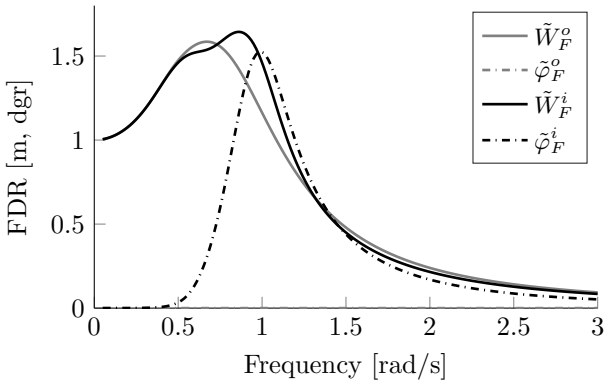

Figure 10: The main peak of the FDR is amplified when $l = 0$.

Although no standing waves can occur at this gap length, the phasing of the reflected wave still results in (anti-)resonance. The resulting peak is slightly higher than the one in open water and is shifted to a higher frequency.

With this the analysis of the body's response excited by the harmonic force is concluded.

5.2. Excitation by the moment

Next the response caused by the external moment is studied. Since the coupling terms are the same ($\tilde{\varphi}_F = \tilde{W}_M$) $\tilde{W}_M$ will not be discussed again so the analysis in this subsection is limited to $\tilde{\varphi}_M$. $\tilde{\varphi}_M$ is shown below using the default set of parameters:

$\tilde{\varphi}_M$ looks qualitatively the same as $\tilde{W}_F$ studied before. The OF is independent of the body so it also applies to an excitation by the moment. The peaks and troughs are

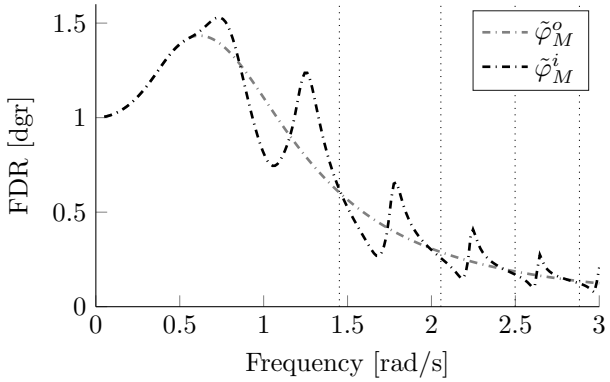

Figure 11: $\tilde{\varphi}_M$ for the default parameters.

again caused by the standing waves in combination with (anti-)resonance. For very small gap lengths the same effects occur as seen in figure 10. The behavior of $\tilde{\varphi}_M$ is qualitatively the same as $\tilde{W}_F$ so no further studies are done.

5.3. Discussion of results

[3] As this study is theoretical, a comparison with relevant model tests is desired. In particular a critical look must be given to the assumption of linearity as model tests have shown that nonlinearities can play an important role for this type of interaction.

[3] In (Toffoli et al., 2015, Nelli et al., 2017) the interaction between a floating elastic plate and incoming monochromatic waves is studied in a two-dimensional wave basin experimental campaign. During these experiments it was observed that for steep waves water can wash on top of the ice floes, a process called overwash (Bennetts et al., 2015). Overwash acts as an amplitude dependent wave energy dissipation mechanism. A comparison of their theoretical model, also based on linear theory, with their experimental results show that the linear model correctly predicts the transmitted amplitudes for low incident steepness. As the steepness increases, overwash starts to play an increasingly important role and consequently the transmitted amplitudes are overpredicted.

[3] As the model presented in this paper is also linear, overwash is not accounted for. Estimating whether it would occur is not possible because the magnitude of the external loads are not based on a physical process and so no quantitative statements can be made about the steepness of the waves. Despite this, some reservations are in order based on their findings. Particularly, the amplified response of the fluid within the gap at the resonance frequencies will be especially susceptible to overwash. As overwash acts as limiting mechanism on the amplitudes of these waves, they might not reach the amplitudes predicted by the linear model. This, in turn, implies that the amplification of the body's response at these frequencies will be lower than those predicted as overwash dissipates energy.

[3] Additionally, when overwash occurs energy can shift to higher harmonics in the reflected wave field and ultimately become irregular all together (Bennetts et al., 2015, Nelli et al., 2017). This effect also disrupts the resonance build-ups observed in this paper. The qualitative results presented in this paper are thus only valid for waves with a low steepness and consequently for relatively small motions of the body.

[3] Lastly, (Nelli et al., 2017) shows that significant drift of the floating plate can occur. Drift forces are not included in the linear model presented in this paper. As the body in this model represents a vessel it would normally have a station-keeping system that would counteract these forces. Even so, the second order wave drift forces act additive to the first order forces studied in this paper and consequently the qualitative results on the effect of the first order forces remain valid.

6. Conclusions and recommendations

In this paper the effects of a nearby level ice sheet on the frequency domain response of a floating body was investigated. Once subjected to an external sinusoidal excitation, the body starts to generate waves that propagate away from it. Those waves falling on ice sheet are partly transmitted into the ice sheet and partly reflected back towards the body. The reflected waves interact with the body, altering its response. How the presence of the ice affects the body's response, i.e., the *ice effect*, was studied in this paper using a 2D model. Based on the numerical results presented the following conclusions can be drawn.

Below a certain *onset frequency* the waves reflected by the ice sheet are negligible and consequently the body does not feel the presence of the ice. Above the onset frequency the ice effect is proportional to the response of the body in open water. Consequently, the susceptibility of a body to the ice effect can be estimated by checking how much of its open water response occurs above or below the onset frequency.

Above the onset frequency the waves reflected by the ice have a pronounced effect on the response of the floater. Quasi-standing waves can occur within the gap between ice and body in certain frequency ranges. Within certain frequency ranges, of which there are infinitely many, half the wavelength of the propagating surface wave of the water layer is approximately an integer multiple of the gap length causing the amplitude of these standing waves to be greatly amplified. Increasing the gap length reduces the spacing (in frequency) of these ranges, i.e. they occur at more frequencies.

Within these ranges the response of the body is significantly altered. Depending on the phasing between the reflected waves and the body's motions resonance or anti-resonance can occur. Even when there is no gap between ice and body the amplitude of the body can still be amplified and its natural frequency somewhat shifted.

Changes in the ice thickness have a significant influence on onset frequency while changes in the Young's modules of the ice and the water depth do not. Lower thicknesses increase the onset frequency. Increasing the mass of the body reduces the magnitude of the ice effect.

Acknowledgements

This work was supported by the SAMCoT CRI through the Research Council of Norway and all of the SAMCoT Partners. The authors would also like to thank the Wikiwaves.org website for providing a good open-source reference for hydroelastic problems involving ice.

Appendix A. Derivation of $\tilde{\phi}_{\mathrm{p},\alpha}$

In this appendix $\tilde{\phi}_{\mathrm{p},\alpha}(x,z)$ is derived. The problem statement is given in section 2.2. The inverse Fourier transform from k to x which arises will be carried out using contour integration.

For the derivation in this appendix and the subsequent ones the following Fourier transform and its inverse are used (an equivalent one is used for the transformation from x to wavenumber k):

$$\tilde{f}(\omega) = \mathfrak{F}(f(t)) = \int_{-\infty}^{\infty} f(t)\mathrm{e}^{-\mathrm{i}\omega t}\,\mathrm{d}t \tag{A.1a}$$

$$f(t) = \mathfrak{F}^{-1}(\tilde{f}(\omega)) = \frac{1}{2\pi}\int_{-\infty}^{\infty} \tilde{f}(\omega)\mathrm{e}^{\mathrm{i}\omega t}\,\mathrm{d}t \tag{A.1b}$$

As a first step, the EOM of the fluid, Eq. (3), is transformed to the wavenumber-frequency domain:

$$-k^2\tilde{\tilde{\phi}}_\alpha + \frac{\partial^2\tilde{\tilde{\phi}}_\alpha}{\partial z^2} = 0 \qquad \forall\ z\in(-H,0) \tag{A.2}$$

Solving this ordinary differential equation for $\tilde{\tilde{\phi}}_\alpha$ gives:

$$\tilde{\tilde{\phi}}_\alpha(k,z) = c_1\cosh(kz) + c_2\mathrm{i}\sinh(kz) \qquad \forall\ z\in(-H,0) \tag{A.3}$$

Substituting Eq. (A.3) into the BC at the seabed (Eq. (5)) gives:

$$c_2 = c_1\tanh(kH) \tag{A.4}$$

Substituting this into the expression of $\tilde{\tilde{\phi}}_\alpha$ and rewriting gives:

$$\tilde{\tilde{\phi}}_\alpha = c_1\frac{\cosh(k(z+H))}{\cosh(kH)} = c_1 Z(k,z) \tag{A.5}$$

The BC at the surface, $z=0$, is:

$$\tilde{p}|_{z=0} = \begin{cases}\tilde{P}_\alpha & \forall\ x\in(x_\alpha-\Delta_\mathrm{x}, x_\alpha+\Delta_\mathrm{x}]\\ 0 & \text{otherwise}\end{cases} \tag{A.6}$$

Transforming this equation into the wavenumber-domain gives:

$$-\rho_w b\left(-\omega^2\tilde{\tilde{\phi}}_\alpha + g\frac{\partial\tilde{\tilde{\phi}}_\alpha}{\partial z}\right)\Bigg|_{z=0} = \tilde{P}_\alpha\frac{\mathrm{e}^{-\mathrm{i}k(x_\alpha+\Delta_\mathrm{x})} - \mathrm{e}^{-\mathrm{i}k(x_\alpha-\Delta_\mathrm{x})}}{-ik} \quad \text{(A.7)}$$

where the fluid pressure $\tilde{p}(x)$ is given by Eq. (6). Substituting the previously found expression for $\tilde{\tilde{\phi}}_\alpha$ and solving for the unknown amplitude c_1 gives:

$$c_1 = \frac{\tilde{P}_\alpha}{\rho_w g}\frac{\mathrm{i}}{k}\frac{\mathrm{e}^{-\mathrm{i}k(x_\alpha+\Delta_\mathrm{x})} - \mathrm{e}^{-\mathrm{i}k(x_\alpha-\Delta_\mathrm{x})}}{\omega^2/g - k\tanh(kH)} \quad \text{(A.8)}$$

Finally, the expression for the potential in the (x,z)-domain is obtained using the inverse Fourier transform with respect to the wavenumber k:

$$\tilde{\phi}_\alpha(x,z) = \frac{\mathrm{i}\tilde{P}_\alpha}{\rho_w g}\frac{1}{2\pi}\int_{-\infty}^{\infty}\frac{1}{k}\frac{\mathrm{e}^{\mathrm{i}k(x-(x_\alpha+\Delta_\mathrm{x}))} - \mathrm{e}^{\mathrm{i}k(x-(x_\alpha-\Delta_\mathrm{x}))}}{\omega^2/g - k\tanh(kH)}Z(k,z)\,\mathrm{d}k \quad \text{(A.9)}$$

The basic integral to be taken in order to evaluate Eq. (A.9) is:

$$\tilde{\Phi}(\hat{x},z) = \frac{\mathrm{i}\tilde{P}_\alpha}{\rho_w g}\frac{1}{2\pi}\int_{-\infty}^{\infty}\frac{1}{k}\frac{\mathrm{e}^{\mathrm{i}k\hat{x}}Z(k,z)}{\omega^2/g - k\tanh(kH)}\,\mathrm{d}k \quad \text{(A.10)}$$

The solution to the original problem can then be obtained using:

$$\tilde{\phi}_\alpha(x,z) = \tilde{\Phi}(x-(x_\alpha+\Delta_\mathrm{x}),z,\omega) - \tilde{\Phi}(x-(x_\alpha-\Delta_\mathrm{x}),z,\omega) \quad \text{(A.11)}$$

In order to evaluate the basic integral it will be converted into a contour integral. The original integration range is a line (in the complex k-plane) ranging from $-\infty$ to ∞ along the real axis. To obtain a closed contour C, the original integration range is closed by adding a segment which connects its extremities, i.e. the positive and negative real-valued infinities. This will be done using a semi-circle with infinite radius which will go over either upper or lower half-plane, depending on the sign of $\hat{x}$. Using the residue theorem, the integral can then be represented as a summation of the residues of the integrand evaluated at the poles enclosed in the contour. Before starting with this procedure the following definitions are made:

$$\tilde{\Phi}(\hat{x},z) = \int_{-\infty}^{\infty} I(k)\,\mathrm{d}k = \int_{-\infty}^{\infty}\frac{I_\mathrm{num}(k)}{I_\mathrm{denom}(k)}\,\mathrm{d}k \quad \text{(A.12)}$$

The conversion to a contour integral can only be done if the integral evaluates to zero along the added segment as otherwise the result of the integral would change. This requires the integrand to converge to zero in the limit of $|k| \to \infty$ along the added segment. To assure this, the integrand is analyzed starting with $Z(k,z)$:

$$Z(k,z) = \frac{\exp(k(z+H)) + \exp(-k(z+H))}{\exp(kH) + \exp(-kH)} \quad \text{(A.13)}$$

The extra segments spans one half-plane and so the values k will take on the segment will be complex. The imaginary part of k results in oscillatory behavior bounded between -1 and 1 and so does not effect convergence. For the real part the two extremes are considered: $k \to \pm\infty$. Both numerator and denominator become infinite at those extremes. However, since $z+H \in [0..H] < H$, the numerator is equal or smaller than the denominator, making the amplitude of $Z(z)$ bounded.

As the integrand goes to infinite at its poles, all the poles have to be identified to make sure that the extra segment does not cross any of them:

- k^{-1}: This term generates a single simple pole, namely $k = 0$.
- $(\omega^2/g - k\tanh(kH))^{-1}$: This is the dispersion relation of surface waves. This term generates two simple poles of opposite sign located on the real-axis related to propagating surface waves. In addition, it generates two countably infinite sets of simple poles of opposite sign located on the imaginary axis which have an accumulation point at $\pm i\infty$. However, as all poles fall inside the proposed contour, the contour does not cross them and so the accumulation point does not influence the convergence.
- $\cosh^{-1}(kH)$: This term does not generate poles because its zeros are negated by the cosine inside the tangent hyperbolic.

Lastly, the exponent is analyzed. Its dependence on x dictates which half-plane has to be used:

$$\lim_{k\to\infty}\mathrm{e}^{\mathrm{i}k\hat{x}} = 0 \;\to\; \begin{cases} C \text{ closes over UHP} & \text{if } \hat{x} > 0 \\ C \text{ closes over LHP} & \text{if } \hat{x} < 0 \end{cases} \quad \text{(A.14)}$$

where LHP and UHP mean the lower and upper half-plane. Even for the special case when $x = 0$ the integrand still converges to zero since the integrand is proportional to $1/k^2$ when $|k| \to \infty$. This means that the integrand converges unconditionally as long as the correct half-planes is used.

Since the integral converges to zero along the added segment it can be added to the integration path without changing the result of the integral. The obtained contour

integral is now evaluated using Cauchy's integral formula:

$$\oint_C I(k)\,dk = \begin{cases} 2\pi\mathrm{i}\sum_{\text{poles in UHP}} \operatorname{Res} I(k_n) & \text{if } \hat{x} > 0 \\ -2\pi\mathrm{i}\sum_{\text{poles in LHP}} \operatorname{Res} I(k_n^-) & \text{if } \hat{x} < 0 \end{cases}$$
$$= \begin{cases} 2\pi\mathrm{i}\sum_{n=0}^{\infty} \gamma_n \left.\frac{I_{\text{num}}(k)}{I'_{\text{denom}}(k)}\right|_{k=k_n} & \text{if } \hat{x} > 0 \\ -2\pi\mathrm{i}\sum_{n=0}^{\infty} \gamma_n \left.\frac{I_{\text{num}}(k)}{I'_{\text{denom}}(k)}\right|_{k=k_n^-} & \text{if } \hat{x} < 0 \end{cases} \tag{A.15}$$

where k_n^- are the roots located in the LHP and k_n those in the UHP. k_n is defined as follows:

- k_0: 0 (generated by the rectangular shape of the pressure element)
- k_1: the negative real pole (propagating mode) of the $\omega^2/g - k\tanh(kH)$ where the Sommerfeld radiation condition was used to eliminate the positive real pole
- $k_n, n \geq 2$: the imaginary poles (evanescent modes) located in the UHP from $\omega^2/g - k\tanh(kH)$ in ascending order

Since the dispersion relation $\omega^2/g - k\tanh(kH)$ is an even function in k, its poles are mirrored in the real and imaginary axis. This implies that its poles in the LHP are minus the poles in the UHP and so $k_n^- = -k_n$. Lastly, since the first pole ($k = 0$) falls on integration part it has to be excluded using Cauchy principal value. To this end a semi-circle with an infinitesimal radius is used. γ_n is introduced to account for the contribution of $k = 0$ which is half compared to the poles that fall inside the contour:

$$\gamma_n = \begin{cases} 1/2, & \text{if } n = 0 \\ 1, & \text{if } n > 0 \end{cases} \tag{A.16}$$

The derivative of the denominator in Eq. (A.15) is given by:

$$I'_{\text{denom}}(k) = \frac{\partial}{\partial k}\left(k(\omega^2/g - k\tanh(kH))\right)$$
$$= \left(\omega^2/g - k\tanh(kH)\right)$$
$$- k\left(kH\operatorname{sech}^2(kH) + \tanh(kH)\right) = Q(k) \tag{A.17}$$

Combining all these results Eq. (A.10) becomes:

$$\tilde{\Phi}(\hat{x}, z, \omega) =$$
$$-\frac{P}{\rho_w g}\begin{cases} \sum_{n=0}^{\infty} \gamma_n Q^{-1}(k_n)\mathrm{e}^{\mathrm{i}k_n\hat{x}} Z(k_n, z), & \text{if } \hat{x} > 0 \\ -\sum_{n=0}^{\infty} \gamma_n Q^{-1}(-k_n)\mathrm{e}^{-\mathrm{i}k_n\hat{x}} Z(-k_n, z), & \text{if } \hat{x} < 0 \end{cases} \tag{A.18}$$

where κ_n was replaced by $-k_n$. Since both $Q(k)$ and $Z(k, z)$ are even functions in k this equation can be further simplified to:

$$\tilde{\Phi}(\hat{x}, z, \omega) = -\frac{P}{\rho_w g}\operatorname{sgn}(\hat{x})\sum_{n=0}^{\infty} \gamma_n Q^{-1}(k_n)\mathrm{e}^{\mathrm{i}k_n|\hat{x}|} Z(k_n, z) \tag{A.19}$$
$$= -\frac{P}{\rho_w g}\operatorname{sgn}(\hat{x})\sum_{n=0}^{\infty} \gamma_n Q_n^{-1}\mathrm{e}^{\mathrm{i}k_n|\hat{x}|} Z_n(z) \tag{A.20}$$

Using this result $\tilde{\phi}_\alpha(x, z)$ can be constructed using Eq. (A.10) which results in:

$$\tilde{\phi}_{\mathrm{p},\alpha}(x, z) = -\frac{\tilde{P}_\alpha}{\rho_w g}\sum_{n=0}^{N} \gamma_n Q_n^{-1} I_{n,\alpha}(x) Z_n(z) \tag{A.21}$$

where $I_{n,\alpha}(x)$ is given by:

$$I_{n,\alpha}(x) = \operatorname{sgn}(x_1(x))\,\mathrm{e}^{\mathrm{i}k_n|x_1(x)|} - \operatorname{sgn}(x_2(x))\,\mathrm{e}^{\mathrm{i}k_n|x_2(x)|} \tag{A.22}$$

where $x_1(x) = x - (x_\alpha + \Delta_\mathrm{x})$ and $x_2(x) = x - (x_\alpha - \Delta_\mathrm{x})$.

It is important to note that k_0 only contributes to the domain $x_\alpha - \Delta_\mathrm{x} < x \leq x_\alpha + \Delta_\mathrm{x}$. When considering the summed effect of all elements this limits the effect of k_0 to $(0, L]$. This is important when the orthogonality of the modes is considered when resolving the interface between ice and water in Appendix D. This is because the interface is located at $x = -l$ and thus falls outside $(0, L]$, making the contribution of k_0 to disappear.

This concludes the derivation of the fluid response $\tilde{\phi}_{\mathrm{p},\alpha}(x, z)$ to the excitation of pressure element α.

Appendix B. Derivation of $\tilde{\phi}_{\mathrm{r},\alpha}$

The derivation of $\tilde{\phi}_{\mathrm{r},\alpha}$ is very similar to that of $\tilde{\phi}_{\mathrm{p},\alpha}$. All governing equations are the same except for the BC at the surface and so its derivation can start from Eq. (A.5):

$$\tilde{\tilde{\phi}}_{r,\alpha} = a_\alpha Z(k, z) \tag{B.1}$$

where a_α is the unknown amplitude. The external forcing in Eq. (7) caused by the pressure element has already been accounted for by $\tilde{\phi}_{\mathrm{p},\alpha}$ and so $\tilde{\phi}_{\mathrm{r},\alpha}$ must satisfy the pressure release condition at its surface, i.e. $p = 0$. This results in the same dispersion relation in the (k, z, ω)-domain:

$$-\omega^2 + gk\tanh(kH) = 0 \tag{B.2}$$

This equation is again solved for k resulting in the same set of roots k_n as found in section Appendix A with the exception that n now starts at 1 due to the absence of the pressure element. Based on this the expression for the reflected potential becomes:

$$\tilde{\phi}_{\mathrm{r},\alpha} = \sum_{n=1}^{N} a_{n,\alpha}\mathrm{e}^{\mathrm{i}k_n(x+l)} Z_n(z)$$
$$\forall\ x \in [-l, \infty)\ \cap\ z \in [-H, 0] \tag{B.3}$$

where the modal amplitudes $a_{n,\alpha}$ are still unknown and the plus in the exponent is due to all the waves having to propagate away from the ice-water interface and this potential being restricted to the right side of the interface ($x > -l$).

Appendix C. Derivation of $\tilde{\phi}_{\mathbf{t},\boldsymbol{\alpha}}$

Apart from the BC at the surface all other equations are the same as in the previous section and so the transmitted potential $\tilde{\phi}_{\mathrm{t},\alpha}$ starts off with the same expression as before:

$$\tilde{\bar{\phi}}_{t,\alpha} = \bar{a}_\alpha Z(k,z) \tag{C.1}$$

where the overbar will be used to differentiate terms related to the ice region from those related to the open water region. For this potential the BC at the surface (Eq. (7)) simplifies to the following:

$$-\omega^2 \rho_i A \tilde{w} + EI \frac{\partial^4 \tilde{w}}{\partial x^4} = \tilde{p}|_{z=0} \tag{C.2}$$

Using Eq. (9) to express $\tilde{w}$ in terms of $\tilde{\phi}_{\mathrm{t},\alpha}$ and using Eq. (6) for the fluid pressure this BC results in the following dispersion relation after transforming to the wavenumber-domain:

$$\bar{a}_\alpha \left(-\omega^2 \rho_i A + EIk^4 + \rho_w g - \rho_w b \frac{\omega^2}{\lambda(k)} \right) \lambda(k) = 0 \tag{C.3}$$

where $\lambda(k) = Z'(k,0) = k \tanh(kH)$. This dispersion relation is solved for k resulting in a countable set of roots $\bar{k}_m$ which is defined as:

- $\bar{k}_{1,2}$: the complex poles located in the upper half-plane which are related to the bending modes of the beam
- $\bar{k}_3$: the negative real pole (propagating fluid mode) related to the free surface where the Sommerfeld radiation condition was used to eliminate the positive real pole
- $\bar{k}_m, m \geq 4$: the countable set of imaginary poles (evanescent fluid modes) from the upper half-plane in ascending order

Based on this, the transmitted potential becomes:

$$\tilde{\phi}_{\mathrm{t},\alpha} = \sum_{m=1}^{M} \bar{a}_{m,\alpha} \mathrm{e}^{-\mathrm{i}\bar{k}_m(x+l)} \bar{Z}_m(z) \qquad \forall\ x \in (-\infty, -l] \ \cap\ z \in [-H, 0] \tag{C.4}$$

where the infinite summation was truncated at M for practical reasons, the modal amplitudes $\bar{a}_{m,\alpha}$ are still unknown, the minus in the exponent ensures that all waves propagate away from the interface and lastly $\bar{Z}_m(z) = Z(\bar{k}_m, z)$.

Appendix D. Resolving the interface at $x = -l$

In this appendix the IC between the open water and the ice covered region is resolved. When the waves caused by the pressure elements arrive at the ice some will be reflected back, generating the reflected potential $\tilde{\phi}_{\mathrm{r},\alpha}$ and some will be transmitted into the ice covered domain, generating the transmitted potential $\tilde{\phi}_{\mathrm{t},\alpha}$. An illustration of the problem to be solved is given in figure 4.

The three potentials derived in the previous appendices satisfy all conditions except the IC at $x = -l$. At this location the following two beam-related stress-free boundaries apply at $z = 0$:

$$EI \frac{\partial^3 \tilde{\phi}_{\mathrm{t},\alpha}}{\partial z x^2}\bigg|_{x=-l,z=0} = 0 \quad \rightarrow \quad \sum_{m=1}^{M} \bar{a}_m \bar{k}_m^2 \bar{\lambda}_m = 0 \tag{D.1a}$$

$$EI \frac{\partial^4 \tilde{\phi}_{\mathrm{t},\alpha}}{\partial z x^3}\bigg|_{x=-l,z=0} = 0 \quad \rightarrow \quad \sum_{m=1}^{M} \bar{a}_m \bar{k}_m^3 \bar{\lambda}_m = 0 \tag{D.1b}$$

where $\bar{\lambda}_m = \lambda(\bar{k}_m) = \bar{k}_m \tanh(\bar{k}_m H)$.

In addition, for $z \in (-H, 0)$ the ICs between the fluid regions need to be satisfied, Eq. (12). They ensure a continuity of horizontal displacements and (linearized) pressure throughout the water column:

$$\frac{\partial \tilde{\phi}_{\mathrm{t},\alpha}}{\partial x}\bigg|_{x=-l} = \left(\frac{\partial \tilde{\phi}_{\mathrm{r},\alpha}}{\partial x} + \frac{\partial \tilde{\phi}_{\mathrm{p},\alpha}}{\partial x} \right)\bigg|_{x=-l} \tag{D.2a}$$

$$-\rho_w b \left(-\omega^2 \tilde{\phi}_{\mathrm{t},\alpha} + g \frac{\partial \tilde{\phi}_{\mathrm{t},\alpha}}{\partial z} \right)\bigg|_{x=-l} = -\rho_w b \left(-\omega^2 \left(\tilde{\phi}_{\mathrm{r},\alpha} + \tilde{\phi}_{\mathrm{p},\alpha} \right) + g \left(\frac{\partial \tilde{\phi}_{\mathrm{r},\alpha}}{\partial z} + \frac{\partial \tilde{\phi}_{\mathrm{p},\alpha}}{\partial z} \right) \right)\bigg|_{x=-l} \tag{D.2b}$$

Through the Laplace equation (Eq. (3)), enforcing a continues horizontal displacements also guarantees a continuity of vertical displacements. From this it follows that the *hydrostatic* pressure terms in Eq. (D.2b), $-\rho_w b g \frac{\partial \tilde{\phi}}{\partial z}$, are already continues across the interface. Next, the remaining *hydrodynamic* pressure terms are proportional to the potentials themselves (after applying a Fourier transform from time to frequency) and so a continuity of potentials themselves will ensure a continuity of fluid pressure. Therefore Eq. (D.2b) will be satisfied when the following simpler condition is satisfied:

$$\tilde{\phi}_{\mathrm{t},\alpha}\Big|_{x=-l} = (\tilde{\phi}_{\mathrm{r},\alpha} + \tilde{\phi}_{\mathrm{p},\alpha})\Big|_{x=-l} \tag{D.3}$$

To satisfy these two equations the orthogonality property of the depth Eigen function $Z_n(z)$ will be used. To do this, both sides of Eq. (D.2a) and (D.3) are multiplied by $Z_j(z)$, where all k_j satisfy the dispersion relation

in Eq. (B.2), and then integrated along z from $-H$ to 0. Noting again that the contribution of k_0 is zero when $x \notin (0, L]$ and that the interface falls outside this region (see Figure 4), k_0 will not contribute to the evaluation of $\tilde{\phi}_{\mathrm{p},\alpha}$ at $x = -l$. Consequently, all remaining N modes of $\tilde{\phi}_{\mathrm{p},\alpha}$ satisfy the dispersion equation in Eq. (B.2) and will therefor be orthogonal to $Z_j(z)$. The procedure will first be applied to Eq. (D.2a):

$$\sum_{m=1}^{M} \bar{a}_{m,\alpha} \frac{\bar{\lambda}_m - \lambda_j}{\bar{k}_m^2 - k_j^2}(-i\bar{k}_m) = \sum_{n=1}^{N} a_{n,\alpha} \frac{\lambda_n - \lambda_j}{k_n^2 - k_j^2}(ik_n) - \frac{\tilde{P}_\alpha}{\rho_w g} \sum_{n=1}^{N} Q_n^{-1} I'_{n,\alpha}(-l) \frac{\lambda_n - \lambda_j}{k_n^2 - k_j^2} \qquad \forall\ j = 1 \,..\, N \tag{D.4}$$

where the summation over N starts at 1 to skip k_0, $\lambda_n = \lambda(k_n)$ and $I'_{n,\alpha}(-l) = -ik_n I_{n,\alpha}(-l)$. Since $\lambda_n = \lambda_j = \omega^2/g$, see Eq. (B.2), the right hand side of Eq. (D.4) is zero unless $n = j$ and so the summation on the right hand side disappears:

$$\sum_{m=1}^{M} \bar{a}_{m,\alpha} \frac{\bar{\lambda}_m - \lambda_j}{\bar{k}_m^2 - k_j^2}(-i\bar{k}_m) = - \frac{Q_j}{2k_j^2}(ik_j) \left(a_{j,\alpha} + \frac{\tilde{P}_\alpha}{\rho_w g} Q_j^{-1} I_{j,\alpha}(-l) \right) \tag{D.5}$$

$$\forall\ j = 1 \,..\, N \tag{D.6}$$

where $\lim_{k_n \to k_j} (\lambda_n - \lambda_j)(k_n^2 - k_j^2)^{-1} = (k_n H \operatorname{sech}^2(k_n H) + \tanh(k_n H))(2k_j)^{-1} = -Q_j\ (2k_j^2)^{-1}$. Since now all roots satisfy the dispersion relation given by Eq. (B.2) (previously k_0 did not) Q_n, given in Eq. (A.17), simplifies to:

$$Q_n = -k_n \left(k_n H \operatorname{sech}^2(k_n H) + \tanh(k_n H) \right) \qquad \forall\ n > 0 \tag{D.7}$$

The same procedure is now applied to the IC prescribing a continuity of potentials, Eq. (D.3), resulting in:

$$\sum_{m=1}^{M} \bar{a}_{m,\alpha} \frac{\bar{\lambda}_m - \lambda_j}{\bar{k}_m^2 - k_j^2} = - \frac{Q_j}{2k_j^2} \left(a_{j,\alpha} - \frac{\tilde{P}_\alpha}{\rho_w g} Q_j^{-1} I_{j,\alpha}(-l) \right) \qquad \forall\ j = 1 \,..\, N \tag{D.8}$$

Eq. (D.8) is now multiplied by $-ik_j$ and added to Eq. (D.5) to get the final expression for the ICs of the fluids:

$$\sum_{m=1}^{M} \bar{a}_{m,\alpha} \frac{\bar{\lambda}_m - \lambda_j}{\bar{k}_m - k_j} = \frac{\tilde{P}_\alpha}{\rho_w g} \frac{I_{j,\alpha}(-l)}{k_j} \qquad \forall\ j = 1 \,..\, N \tag{D.9}$$

This gives N equations to be satisfied. Together with the two equations from the beam's BCs, Eq. (8), a total of $N + 2$ equations need to be satisfied. This means $N + 2$ unknown $\bar{a}_m$'s are needed and so $M = N + 2$. The overall number of modes, given by N, will be determined later based on the convergence of the model's output. Once the linear problem for $\bar{a}_{m,\alpha}$ has been solved the unknown amplitude $a_{n,\alpha}$ are easily obtained using:

$$a_{n,\alpha} = -\frac{2k_n^2}{Q_j} \sum_{m=1}^{M} \bar{a}_{m,\alpha} \frac{\bar{\lambda}_m - \lambda_n}{\bar{k}_m^2 - k_n^2} + \frac{\tilde{P}_\alpha}{\rho_w g} Q_n^{-1} I_{n,\alpha}(-l) \qquad \forall\ n = 1 \,..\, N \tag{D.10}$$

The amplitudes of the transmitted and reflected potentials have now been obtained. The combined effect of all three potentials gives the response due to the excitation of a single pressure element α, including the effects of the ice covered region.

References

L. G. Bennetts, A. Alberello, M. H. Meylan, C. Cavaliere, A. V. Babanin, and A. Toffoli. An idealised experimental model of ocean surface wave transmission by an ice floe. *Ocean Modelling*, 96:85–92, 2015. ISSN 14635003. doi: 10.1016/j.ocemod.2015.03.001. URL http://dx.doi.org/10.1016/j.ocemod.2015.03.001.

H. Chung and C. M. Linton. Reflection and transmission of waves across a gap between two semi-infinite elastic plates on water. *Quarterly Journal of Mechanics and Applied Mathematics*, 58(1): 1–15, 2005. ISSN 00335614. doi: 10.1093/qjmamj/hbh011.

C. Fox and V. A. Squire. Reflection and transmission characteristics at the edge of shore fast sea ice. *Journal of Geophysical Research*, 95(C7):11629, 1990. ISSN 0148-0227. doi: 10.1029/JC095iC07p11629. URL http://doi.wiley.com/10.1029/JC095iC07p11629.

C. Fox and V. A. Squire. On the oblique reflexion and transmission of ocean waves at shore fast sea ice. *Philosophical Transactions of the Royal Society A*, 347(1682): 185–218, 1994. ISSN 1364-503X. doi: 10.1098/rsta.1994.0044. URL http://rsta.royalsocietypublishing.org/cgi/doi/10.1098/rsta.1994.0044.

R. E. Gagnon. Results of numerical simulations of growler impact tests. *Cold Regions Science and Technology*, 49:206–214, 2007. ISSN 0165-232X. doi: http://dx.doi.org/10.1016/j.coldregions.2007.03.016. URL http://www.sciencedirect.com/science/article/pii/S0165232X07000754.

R. E. Gagnon and J. Wang. Numerical simulations of a tanker collision with a bergy bit incorporating hydrodynamics, a validated ice model and damage to the vessel. *Cold Regions Science and Technology*, 81:26–35, sep 2012. ISSN 0165232X. doi: 10.1016/j.coldregions.2012.04.006. URL http://linkinghub.elsevier.com/retrieve/pii/S0165232X12000870.

F. B. Jensen, W. A. Kuperman, M. B. Porter, and H. Schmidt. *Computational Ocean Acoustics*. Springer New York, New York, NY, 2011. ISBN 978-1-4419-8677-1. doi: 10.1007/978-1-4419-8678-8. URL http://link.springer.com/10.1007/978-1-4419-8678-8.

F. Montiel, L. G. Bennetts, and V. A. Squire. The transient response of floating elastic plates to wavemaker forcing in two dimensions. *Journal of Fluids and Structures*, 28:416–433, 2012. ISSN 08899746. doi: 10.1016/j.jfluidstructs.2011.10.007. URL http://dx.doi.org/10.1016/j.jfluidstructs.2011.10.007.

F. Nelli, L. G. Bennetts, D. M. Skene, J. P. Monty, J. H. Lee, M. H. Meylan, and A. Toffoli. Reflection and transmission of regular water waves by a thin, floating plate. *Wave Motion*, 70:209–221, 2017. ISSN 01652125. doi: 10.1016/j.wavemoti.2016.09.003. URL http://dx.doi.org/10.1016/j.wavemoti.2016.09.003.

A. Palmer and K. Croasdale. *Arctic Offshore Engineering*. 2013. ISBN 978-981-4368-77-3.

V. Squire. Of Ocean Waves and Sea Ice. *Annual Review of Fluid Mechanics*, 27(1):115–168, 1995. ISSN 00664189. doi: 10.1146/annurev.fluid.27.1.115. URL http://fluid.annualreviews.org/cgi/doi/10.1146/annurev.fluid.27.1.115.

V. Squire. Of ocean waves and sea-ice revisited. *Cold Regions Science and Technology*, 49(2):110–133, aug 2007. ISSN 0165232X. doi: 10.1016/j.coldregions.2007.04.007. URL http://linkinghub.elsevier.com/retrieve/pii/S0165232X07000870.

J. J. Stoker. *Water Waves*. John Wiley & Sons, Inc., Hoboken, NJ, USA, jan 1992. ISBN 9781118033159. doi: 10.1002/9781118033159. URL http://doi.wiley.com/10.1002/9781118033159.

B. Su, K. Riska, and T. Moan. A numerical method for the prediction of ship performance in level ice. *Cold Regions Science and Technology*, 60(3):177–188, 2010. ISSN 0165232X. doi: 10.1016/j.coldregions.2009.11.006. URL http://dx.doi.org/10.1016/j.coldregions.2009.11.006.

G. W. Timco and W. F. Weeks. A review of the engineering properties of sea ice. *Cold Regions Science and Technology*, 60(2):107–129, 2010. ISSN 0165232X. doi: 10.1016/j.coldregions.2009.10.003. URL http://dx.doi.org/10.1016/j.coldregions.2009.10.003.

A. Toffoli, L. G. Bennetts, M. H. Meylan, C. Cavaliere, A. Alberello, J. Elsnab, and J. P. Monty. Sea ice floes dissipate the energy of steep ocean waves. *Geophysical Research Letters*, 42(20):8547–8554, 2015. ISSN 19448007. doi: 10.1002/2015GL065937.

A. Tsarau, R. Lubbad, and S. Løset. A numerical model for simulation of the hydrodynamic interactions between a marine floater and fragmented sea ice. *Cold Regions Science and Technology*, 103:1–14, 2014. ISSN 0165232X. doi: 10.1016/j.coldregions.2014.03.005.

P. Valanto. The resistance of ship in level ice. *Transactions of the Society of Naval Architects and Marine Engineers*, 109:53–83, 2001.

T. D. Williams and V. A. Squire. The effect of submergence on wave scattering across a transition between two floating flexible plates. *Wave Motion*, 45(3):361–379, 2008. ISSN 01652125. doi: 10.1016/j.wavemoti.2007.07.003.

B. Wright. Ice loads on the Kulluk in managed ice conditions. In *Proceedings of the 16 th International Conference on Port and Ocean Engineering under Arctic Conditions*, page 553, 2001.